



Unusual $S=1$ Four-Coordinate Fe(IV) Complexes Supported by Bisamide Ligands: Syntheses, Characterization, and Electronic Structures

Bufan Zhang, Justin P. Joyce, Nikki J. Wolford, William W. Brennessel, Serena DeBeer, and Michael L. Neidig*

Abstract: The catalytic relevance of Fe(IV) species in non-heme iron catalysis has motivated synthetic advances in well-defined five- and six-coordinate Fe(IV) complexes for a better understanding of their fundamental electronic structures and reactivities. Herein, we report the syntheses of FeDipp₂ and FeMes₂, a pair of unusual four-coordinate non-heme formally Fe(IV) complexes with $S=1$ ground states supported by strongly donating bisamide ligands. By combining spectroscopic characterization and computational modeling, we found that small variations in ligand aryl substituents resulted in substantial changes in both structures and bonding. This work highlights the strong donor capabilities and modularity of the bisamide ligand set. More broadly, it is a critical contribution to the utilization of ligand design to modulate molecular geometries and electronic structures of low-coordinate, high-valent iron complexes.

Non-heme iron catalysis encompasses a wide range of biologically important transformations, including O₂/H₂ activation,^[1–2] oxidative C–H activation/functionalization,^[3] and ammonia synthesis.^[4] In these reactions, high-valent iron species are often proposed and/or experimentally

observed as key reactive intermediates.^[5–6] Motivated by the ubiquitous involvement of Fe(IV) species in non-heme molecular catalysis, a plethora of well-defined Fe(IV) complexes have been reported over the last 20 years.^[7–11] These synthetic advances provide valuable opportunities for spectroscopic characterizations, as well as empirical basis for computational modeling of electronic structures and bonding to facilitate our understanding of reaction mechanisms and reactivities. A wide range of ligands have been utilized to support monomeric Fe(IV) centers, among which multi-dentate nitrogen-donor ligands, including *N*-tetramethyl cyclams (TMCs),^[12–14] tetraamido macrocyclic ligands (TAMLs),^[15–18] tris(pyridylmethyl)amines (TPAs) and their derivatives,^[19–20] as well as 1,1-di(pyridin-2-yl)-*N,N*-bis(pyridin-2-ylmethyl)methanamine (N₄Py),^[21] are the most common.

While many isolable non-heme five- and six-coordinate Fe(IV) complexes have been extensively studied using various spectroscopic techniques, much less is known about the fundamental electronic structures of four-coordinate non-heme Fe(IV) complexes. Many formally Fe(IV) complexes in current literature have been speculated or shown to have significant ferric or ferrous contributions,^[22–24] including a recent example of a disilylhydrazido ligand-supported $S=1$ organoiron complex.^[25] To our knowledge, there are only four examples of bona fide non-heme, four-coordinate Fe(IV) complexes in current literature (Figure 1). Initially reported by Bower and Tennet in 1972,^[26] Fe(1-norbornyl)₄ was not structurally characterized until 2013 by Hayton and co-workers.^[27] A few years later, Fürstner and co-workers reported two additional homoleptic Fe(IV) complexes, Fe(cyclohexyl)₄ and Fe(1-adamantyl)₄.^[28]

[*] Dr. B. Zhang, Dr. N. J. Wolford, Dr. W. W. Brennessel
 Department of Chemistry
 University of Rochester
 Hutchison Hall, 120 Trustee Road, 14627 Rochester, NY,
 United States

Dr. B. Zhang, Dr. J. P. Joyce, Prof. Dr. S. DeBeer
 Department of Inorganic Spectroscopy
 Max Planck Institute for Chemical Energy Conversion
 Stiftstraße 34–36, 45470 Mülheim an der Ruhr, Germany

Prof. Dr. M. L. Neidig
 Department of Chemistry
 University of Oxford
 Inorganic Chemistry Laboratory, South Parks Road,
 OX1 3QR Oxford, United Kingdom
 E-mail: michael.neidig@chem.ox.ac.uk

© 2024 The Authors. Angewandte Chemie International Edition published by Wiley-VCH GmbH. This is an open access article under the terms of the Creative Commons Attribution License, which permits use, distribution and reproduction in any medium, provided the original work is properly cited.

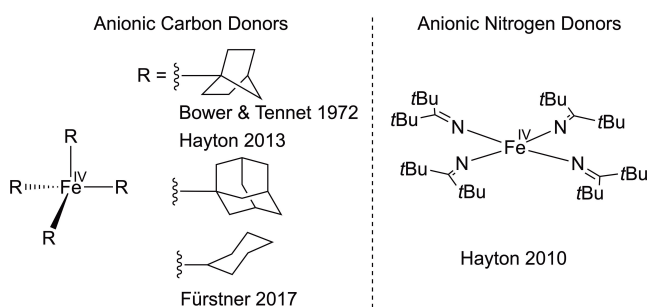


Figure 1. Isolable four-coordinate non-heme Fe(IV) complexes.

All three Fe(IV)-tetraalkyl complexes adopt tetrahedral geometries and exhibit diamagnetic ground states ($S=0$). In sharp contrast, $\text{Fe}(\text{N}=\text{CtBu}_2)_4$ reported by Hayton and co-workers has been the only structurally characterized four-coordinate Fe(IV) complex supported by non-carbanion donor ligands.^[29] While it adopts a highly unusual square planar geometry, $\text{Fe}(\text{N}=\text{CtBu}_2)_4$ is also diamagnetic. So far, there has been no well-characterized examples of four-coordinate Fe(IV) complexes with open-shell configurations.

An important commonality among the examples above is the presence of strongly donating ligands. However, the scarcity of these four-coordinate Fe(IV) complexes has precluded further evaluation of ligand effects on their structures and bonding. We aim to address this limitation by utilizing the bisamide ligand set, whose high modularity and exceptional donor capabilities were shown in our previous work.^[30] Herein, we report the syntheses of FeDipp_2 (**2**) and FeMes_2 (**3**), a pair of unusual $S=1$ non-heme four-coordinate formally Fe(IV) complexes. By combining spectroscopic techniques with computational studies, our results show that modification of ligand aryl substituents resulted in significant structural distortion and fundamentally distinct electronic structures.

To access four-coordinate Fe(IV) complexes, our approach was to synthesize and subsequently oxidize their ferric precursors. To reach the correct coordination number, we chose to use 2.05 equivalents of ligand with respect to the iron precursor. Treatment of FeCl_3 with 2.05 equivalents of DippLi_2 in anhydrous $\text{Et}_2\text{O}/\text{DME}$ (10:1) (DME = dimethoxyethane) inside a N_2 -filled glovebox resulted in a dark purple solution. Dilution with anhydrous pentane followed by cooling to -80°C yielded dark purple crystals, which were confirmed to be $[\text{FeDipp}_2][\text{Li}(\text{DME})_3]$ (**1**) by single crystal X-ray diffraction (SC-XRD) (Figure 2, A).^[31] An isolated yield of 86% was achieved after the reaction conditions were optimized.

1 crystallizes in the monoclinic space group $P2_1/n$. Its geometry is best described as highly distorted tetrahedral, with a $59.28(6)^\circ$ twist angle between the N1-Fe-N2 and the N3-Fe-N4 planes (referred to as ϕ from now on). Its geometry resembles that of $\text{Fe}(\text{pda})_2$ ($\text{pda} = N,N'$ -bis(pentafluorophenyl)-*o*-phenylenediamide), another ferric- N_4 complex supported by bis(α -imine) ligands with a ϕ of 54° .^[32] The average Fe–N bond length of **1** [$1.972(3) \text{ \AA}$] is longer than that found in $\text{Fe}(\text{pda})_2$ (avg. 1.897 \AA), which is consistent with the fact that the former has saturated ligand backbones whereas those of the latter are unsaturated. Zero-field, 80 K ^{57}Fe Mössbauer features a broad doublet with an isomer shift (δ) of 0.27 mm/s and a quadruple splitting ($|\Delta E_{\text{O}}|$) of 1.27 mm/s (Supporting Information, Figure S1). Magnetic susceptibility measurements using the Evans method yielded an effective magnetic moment (μ_{eff}) of $5.9(1) \text{ B.M.}$, consistent with a $S=5/2$ spin state. This was further confirmed by continuous-wave (CW) X-band EPR, which features a $S=5/2$ signal with effective g -values (g') of 6.89 , 5.03 , and 1.96 (Figure 2, B).

As an initial test reaction, we chose O_2 as the oxidant for its convenience. To our delight, exposure of a solution of **1**

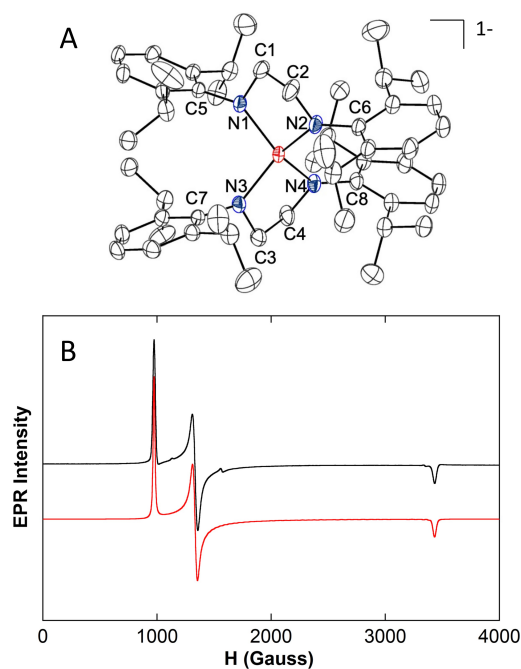
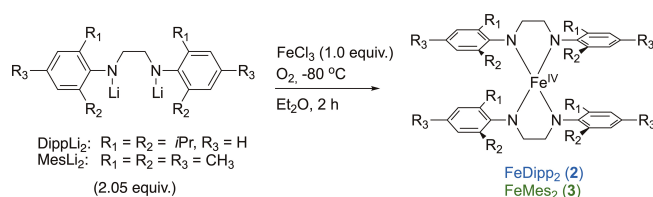


Figure 2. A) X-ray crystal structure of **1**. The $[\text{Li}(\text{DME})_3]^+$ counterion and hydrogen atoms are omitted for clarity. Thermal ellipsoids are at 50% probability. B) CW X-band EPR of **1** in 2-methyl-THF at 10 K (black trace). The spectrum is simulated with an $S=5/2$ spin representation with parameters $g' = [6.89, 5.03, 1.96]$ and 11 G full-width half-maximum (fwhm) Lorentzian line broadening (red trace).

in Et_2O to pure O_2 at -80°C resulted in a color change from dark purple to reddish brown within a minute. After 30 min of standing under a static O_2 atmosphere at -80°C , the reaction yielded dark brown crystals, which were revealed to be **2** by SC-XRD (Figure 3, A).^[31] Subsequently, we found that **2** could also be synthesized via a one-pot protocol, where **1** was generated in situ and treated with O_2 without being isolated. With this method, an isolated yield of 44% was achieved for **2** after the reaction conditions were optimized (Scheme 1).

With a ϕ of $47.03(9)^\circ$, **2** adopts an intermediate geometry between a tetrahedral ($\phi=90^\circ$) and a square-planar ($\phi=0^\circ$). Compared to those in **1** [$1.972(3) \text{ \AA}$], the Fe–N bonds in **2** [$1.861(2) \text{ \AA}$] are contracted by $\sim 0.1 \text{ \AA}$ on average as a result of one-electron oxidation (Table 1). The shortening of the Fe–N bond lengths is consistent with the oxidation of $[\text{Fe}(\text{N}=\text{CtBu}_2)_4][\text{Li}(\text{DME})]$ to $\text{Fe}(\text{N}=\text{CtBu}_2)_4$ reported by Hayton and co-workers (from 1.938 \AA to 1.773 \AA).^[29] The



Scheme 1. Syntheses of **2** and **3** via one-pot in situ oxidation of their respective ferric precursors with O_2 .

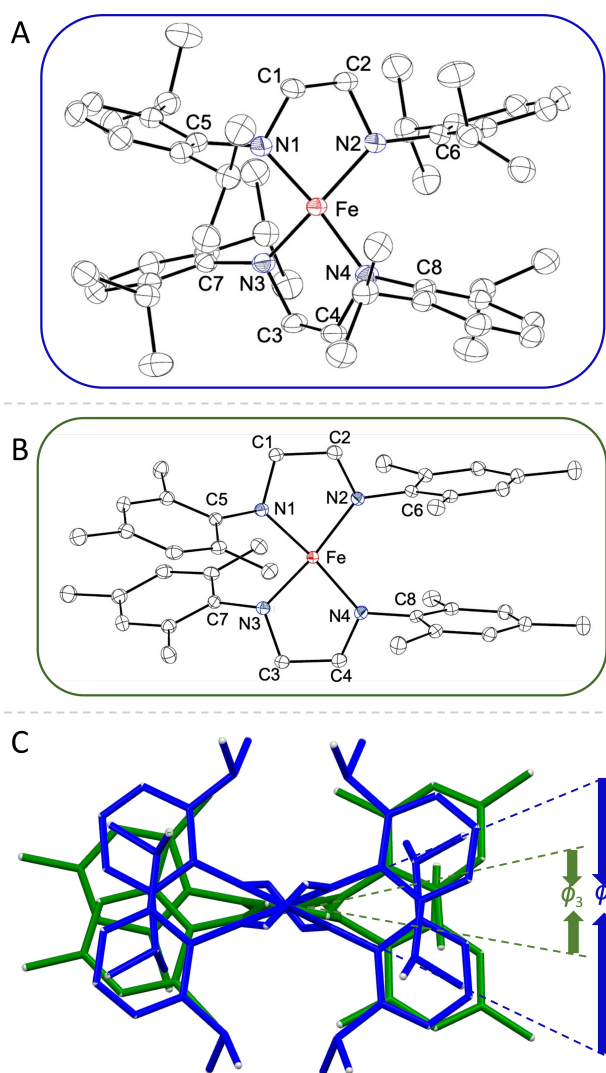


Figure 3. X-ray crystal structures of A) **2** and B) **3**. For both structures, hydrogen atoms are omitted for clarity. Thermal ellipsoids are shown at 50% probability. The labels of the atoms in both complexes here are different from those in the crystal structure reports in the Supporting Information, as they were re-assigned for ease of direct comparison between structures. C) Overlay of crystal structures of **2** and **3** [top view; $\phi_2 = 47.03(9)^\circ$, $\phi_3 = 21.96(3)^\circ$].

longer average Fe–N bond length of **2** compared to that of $\text{Fe}(\text{N}=\text{CtBu}_2)_4$ could be rationalized by the absence of metal-to-ligand back-bonding in **2**. Additionally, compared to $\text{Fe}(\text{N}=\text{CtBu}_2)_4$, in which the two sets of opposing ketimides are nearly linear [$165.5(3)^\circ$ and $166.6(3)^\circ$], **2** exhibits more bent diagonals, with a $148.51(6)^\circ$ angle between the N1–Fe–N4 and N2–Fe–N3 planes. Conversely,

the average Fe–N bond length of **2** is shorter than those reported for various Fe(IV) complexes supported by tetraanionic TAML ligands [avg. Fe–N: $1.902(7)$ Å– $1.910(2)$ Å].^[16] Of note, these Fe(IV)TAML complexes are five- or six-coordinate, as there are no additional examples of isolable four-coordinate Fe(IV) complexes supported by anionic nitrogen donor ligands other than $\text{Fe}(\text{N}=\text{CtBu}_2)_4$. Further, we highlight that the average Fe–N bond length of **2** is also significantly shorter compared to those reported for Fe(II)- and Fe(III)-amide complexes in literature (Supporting Information, Table S6).^[30,33–36]

Motivated by the convenience of accessing **2** via in situ oxidation of **1** with O_2 , we adopted a similar strategy for synthesizing **3** (Scheme 1). Treatment of FeCl_3 with 2.05 equivalents of MesLi_2 in Et_2O resulted in a dark green solution, which instantly turned red upon exposure to anhydrous O_2 at -80°C . Reddish brown crystals suitable for XRD could be isolated at 40% yield via vacuum filtration at -30°C inside a N_2 -filled glovebox. While the crystal structure of **3** (Figure 3, B) is very similar to that of **2** in terms of average Fe–N bond lengths [$1.861(2)$ Å vs. $1.887(2)$ Å] and bisamide ligand bite angles [$85.45(9)^\circ$ vs. $84.03(5)^\circ$], it exhibits two pronounced differences.^[31] First, the replacement of Dipp with Mes in **3** led to a reduction in ϕ from $47.03(9)^\circ$ to $21.96(3)^\circ$ relative to that of **2** (Figure 3, C), resulting in comparable planarity as that of $\text{Fe}(\text{N}=\text{CtBu}_2)_4$, ($\phi = 17^\circ$). Second, **2** and **3** exhibit different intramolecular non-covalent interactions. While four pairs of CH_3 - π interactions (H-to-centroid distances: 2.653 Å and 2.619 Å) are found in the structure of **2**, the structure of **3** exhibits two pairs of CH_3 - π interactions (H-to-centroid distances: 3.049 Å) and one π - π stacking interaction (centroid-centroid distance: 3.637 Å) (Supporting Information, Figure S2).

Magnetic susceptibility measurements using the Evans method yielded μ_{eff} of $2.8(1)$ B.M. and $3.0(1)$ B.M. for **2** and **3**, respectively, both of which are consistent with the $S = 1$ ground states. Zero-field, 80 K ^{57}Fe Mössbauer was then utilized to characterize both complexes in the solid state. The spectrum of **2** features a doublet with the parameters $\delta = 0.00$ mm/s and $|\Delta E_{\text{O}}| = 2.70$ mm/s (Figure 4, A). The significant decrease in the isomer shift of **2** compared to that of **1** (0.27 mm/s) is consistent with the oxidation of the iron center.^[29] Similarly, the Mössbauer spectrum of **3** features a doublet with the parameters $\delta = -0.15$ mm/s and $|\Delta E_{\text{O}}| = 3.00$ mm/s (Figure 4, B). The low isomer shifts of **2** and **3** are consistent with those reported for other ferryl complexes, such as $\text{Fe}(\text{1-norbornyl})_4$ ($\delta = -0.28$ mm/s),^[28] $\text{Fe}(\text{N}=\text{CtBu}_2)_4$ ($\delta = -0.15$ mm/s),^[29] and $[\text{Fe}(\text{TAML})\text{Cl}]^-$ ($\delta = -0.04$ mm/s).^[15] The large $|\Delta E_{\text{O}}|$ values of **2** and **3** are consistent with their distorted planar geometries and triplet ground states.

Table 1: Comparison of selected crystal metrics of **1**, **2**, and **3**.

complex	avg. Fe–N	avg. N–C(sp ²)	avg. N–C(sp ³)	avg. backbone C–C	avg. bisamide bite angle	avg. diagonal N–Fe–N	ϕ
1	$1.972(3)$ Å	$1.415(4)$ Å	$1.463(6)$ Å	$1.517(4)$ Å	$85.54(6)^\circ$	$140.50(7)^\circ$	$59.28(6)^\circ$
2	$1.861(2)$ Å	$1.439(3)$ Å	$1.469(3)$ Å	$1.497(4)$ Å	$85.45(9)^\circ$	$148.51(6)^\circ$	$47.03(9)^\circ$
3	$1.887(2)$ Å	$1.417(2)$ Å	$1.466(3)$ Å	$1.515(2)$ Å	$84.03(5)^\circ$	$164.82(5)^\circ$	$21.96(3)^\circ$

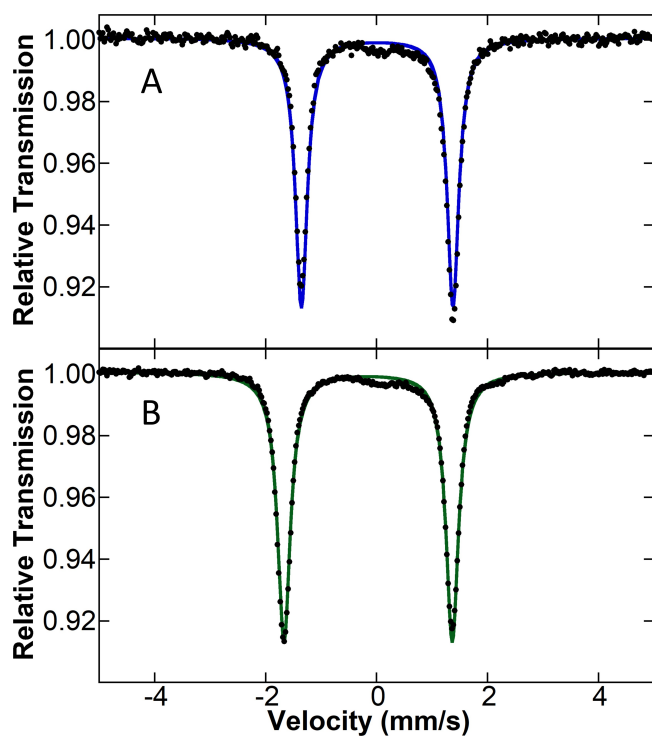


Figure 4. Zero-field, 80 K ^{57}Fe Mössbauer of **2** (A) and **3** (B). Black dotted trace: raw data. Colored solid traces: simulation. Parameters for **2**: $\delta = 0.00$ mm/s, $|\Delta E_Q| = 2.70$ mm/s. Parameters for **3**: $\delta = -0.15$ mm/s, $|\Delta E_Q| = 3.00$ mm/s.

Furthermore, the increase in quadrupole splitting from **2** to **3** is in accordance to the higher planarity of the latter. However, the decrease in isomer shift from 0.00 mm/s (**2**) to -0.15 mm/s (**3**) is unexpected, considering the fact that the average Fe–N bond lengths in **2** and **3** are almost identical. This observation directly contradicts a well-established trend that, for iron complexes with the same spin state and supported by the same type of ligands, more negative isomer shifts are usually correlated with shorter iron-ligand bond lengths.^[37] To shed light on this unusual behavior, we then proceeded to probe the electronic structures of these complexes computationally.

The geometries of **2** and **3** were optimized using several different functionals (PBE0/D3BJ, BP86/D3, B3LPY/D3BJ, R2SCAN/D4) in order for the most suitable level of theory to be selected (Supporting Information, Tables S1–S2). Among those, R2SCAN/D4 yielded structural metrics that were in good agreement with experimental values for both **2** and **3** at the $S=1$ spin state (Supporting Information, Tables S3–S4). These optimized structures were used for subsequent CASSCF/NEVPT2 calculations.

CASSCF (12, 9) calculations on the $S=1$ ground state of **2** and **3** were performed with an active space that included the five 3d orbitals of the Fe-center and the four σ -/ π -donor groups of the amide-lone pairs. The intermediacy of the geometry of **2** between square planar and tetrahedral enables σ -donation from the ligands' $N(\pi)$ orbital to the Fe(d_{xz}) orbitals (Figure 5). Because **2** exhibits minimal multi-reference character, descriptive of the charge-transfer

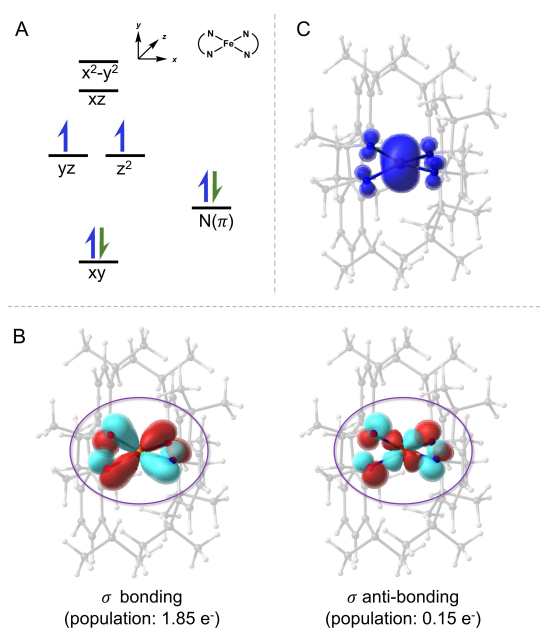


Figure 5. A) Qualitative, truncated molecular orbital (MO) Scheme for **2**. B) σ Bonding and anti-bonding interactions between the Fe(d_{xz}) and the $N(\pi)$ orbitals (σ bonding population: $1.85 e^-$, σ anti-bonding population: $0.15 e^-$). C) Spin density map for the $S=1$ ground state of **2**, where blue and green represent α - and β -character, respectively. In this case, α -character predominates.

character in the σ -type bonding between Fe(d_{xz}) and the amides, its electronic structure is best described as a bona fide Fe(IV) with a $S=1$ ground state.

In stark contrast to **2**, **3** exhibits a more complex bonding behavior. The decrease in ϕ between the two bisamide ligands in **3** changes the type of bonding interaction between the $N(\pi)$ orbital and the Fe(d_{xz}) orbital from σ to π (Figure 6). The 0.15 mm/s decrease in the isomer shift of **3** compared to that of **2** is consistent with their direct relationship to oxidation state reported for Fe π -bonded systems.^[38] Furthermore, the CASSCF (12,9) wavefunction ascribes partial (20%) ligand radical character that is strongly magnetically coupled to an open-shell ferric ($S=3/2$) center. The multireference bonding in **3** that we detail in the Supporting Information is distinct from typical redox non-innocence, where ligands such as bis(iminopyridines),^[39] diazabutadienes,^[40] porphyrins and corroles^[41–42] are antiferromagnetically coupled with their coordinated metal center. We note that while it is common for formally Fe(IV) complexes with ferrous or ferric character to exhibit higher isomer shifts, the -0.15 mm/s isomer shift of **3** is characteristic of a high-valent iron center.^[24–25]

In conclusion, we have accessed a pair of unusual four-coordinate non-heme formally Fe(IV) complexes with triplet ground states. We found that variation in the ligand aryl substituents led to substantial differences in structures and bonding, highlighting the advantageous modularity of the bisamide ligand set. As such, this work represents a critical contribution to tuning molecular geometry and electronic structures of low-coordinate, high-valent iron complexes via ligand modifications, which in turn has a broader, positive

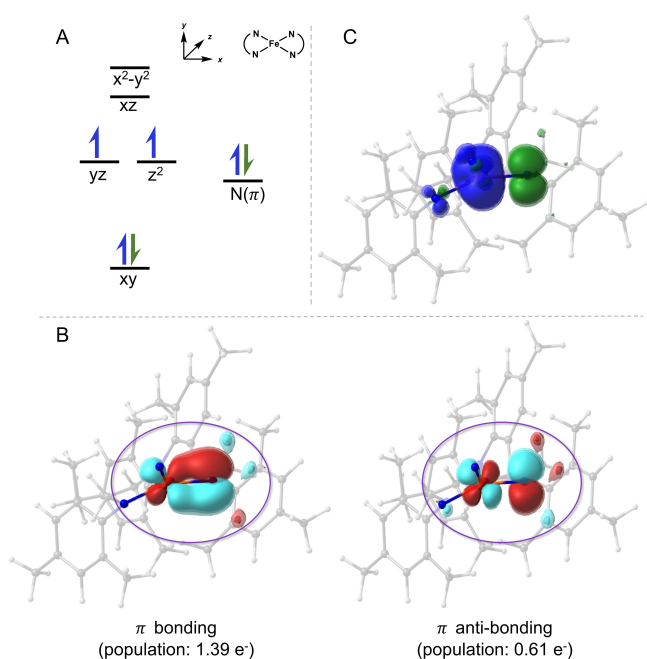


Figure 6. A) Qualitative, truncated MO scheme for **3**. B) π bonding and anti-bonding interactions between the Fe(d_{xz}) and the N(π) orbitals (π bonding population: $1.39 e^-$, π anti-bonding population: $0.61 e^-$). C) Spin density map for the $S=1$ ground state of **3**, where blue and green represent α - and β -character, respectively.

impact on our understanding of the structural-bonding correlation of these unusual complexes as well.

Supporting Information

The authors have cited additional references within the Supporting Information.^[39–46]

Acknowledgements

M. L. N. acknowledges support from the U. S. National Institute of Health (R01 GM 111480) for funding this research. J. P. J. acknowledges support from the Humboldt Foundation. The Max Planck Society is gratefully acknowledged by B. Z., J. P. J. and S. D. for funding.

Conflict of Interest

The authors declare no conflict of interest.

Data Availability Statement

The data that support the findings of this study are available from the corresponding author upon reasonable request.

Keywords: High-Valent • Iron(IV) • Bisamide • Four-Coordinate • Structures

- [1] X. Shan, L. Que Jr. *J. Inorg. Biochem.* **2006**, *100*, 421–433.
- [2] B. Mondal, L. Roy, F. Neese, S. Ye, *Isr. J. Chem.* **2016**, *56*, 763–772.
- [3] K. L. Stone, A. S. Borovik, *Curr. Opin. Chem. Biol.* **2009**, *13*, 114–118.
- [4] C. Van Stappen, L. Decamps, G. E. Cutstail III, R. Bjorsson, J. T. Henthorn, J. A. Birrell, S. Debeer, *Chem. Rev.* **2024**, *120*, 5005–5081.
- [5] J. Hohenberger, K. Ray, K. Meyer, *Nat. Commun.* **2012**, *3*, 720.
- [6] J. T. Groves, *J. Inorg. Biochem.* **2006**, *100*, 434–447.
- [7] J. P. Bigi, W. H. Harman, B. Lassalle-Kaiser, D. M. Robles, T. A. Stich, J. Yano, R. D. Britt, C. J. Chang, *J. Am. Chem. Soc.* **2012**, *134*, 1536–1542.
- [8] S. Hong, H. So, H. Yoon, K. B. Cho, Y. M. Lee, S. Fukuzumi, W. Nam, *Dalton Trans.* **2013**, *42*, 7842–7845.
- [9] K. L. Barnett, M. Vasiliu, T. H. Stein, M. V. Delahay, F. Qu, D. L. Gerlach, D. A. Dixon, K. H. Shaughnessy, *Inorg. Chem.* **2020**, *59*, 5579–5592.
- [10] S. Meyer, I. Klawitter, S. Demeshko, E. Bill, F. Meyer, *Angew. Chem. Int. Ed.* **2013**, *52*, 901–905.
- [11] O. Prakash, P. Chabera, N. W. Rosemann, P. Huang, L. Haggstrom, T. Ericsson, D. Strand, P. Persson, J. Bendix, R. Lomoth, K. Wärnmark, *Chemistry*. **2020**, *26*, 12728–12732.
- [12] J. England, J. O. Bigelow, K. M. Van Heuvelen, E. R. Farquhar, M. Martinho, K. K. Meier, J. R. Frisch, E. Munck, L. Que Jr. *Chem. Sci.* **2014**, *5*, 1204–1215.
- [13] J.-U. Rohde, J.-H. In, M. H. Lim, W. W. Brennessel, M. R. Bukowski, A. Stubna, E. Münck, W. Nam, L. Que Jr, *Science*. **2003**, *299*, 1037–1039.
- [14] A. Zhou, J. Prakash, G. T. Rohde, J. E. Klein, S. T. Kleespies, A. Draksharapu, R. Fan, Y. Guo, C. J. Cramer, L. Que Jr. *Inorg. Chem.* **2017**, *56*, 518–527.
- [15] T. J. Collins, *Acc. Chem. Res.* **2002**, *35*, 782–790.
- [16] A. Chanda, D. L. Popescu, F. Tiago De Oliveira, E. L. Bominaar, A. D. Ryabov, E. Münck, T. J. Collins, *J. Inorg. Biochem.* **2006**, *100*, 606–619.
- [17] T. J. Collins, A. D. Ryabov, *Chem. Rev.* **2017**, *117*, 9140–9162.
- [18] X. X. Li, X. Lu, J. W. Park, K. B. Cho, W. Nam, *Chemistry*. **2021**, *27*, 17495–17503.
- [19] M. H. Lim, J.-U. Rohde, A. Stubna, M. R. Bukowski, M. Costas, R. Y. Ho, E. Münck, W. Nam, L. Que Jr. *Proc. Natl. Acad. Sci. USA* **2003**, *100*, 3665–3670.
- [20] M. Kodera, Y. Kawahara, Y. Hitomi, T. Nomura, T. Ogura, Y. Kobayashi, *J. Am. Chem. Soc.* **2012**, *134*, 13236–13239.
- [21] J. Kaizer, E. J. Klinker, N. Y. Oh, J.-U. Rohde, W. J. Song, A. Stubna, J. Kim, E. Münck, W. Nam, L. Que Jr. *J. Am. Chem. Soc.* **2004**, *126*, 472–473.
- [22] B. P. Jacobs, P. T. Wolczanski, Q. Jiang, T. R. Cundari, S. N. Macmillan, *J. Am. Chem. Soc.* **2017**, *139*, 12145–12148.
- [23] T. Betley, J. C. Peters, *J. Am. Chem. Soc.* **2004**, *126*, 6252–6254.
- [24] S. M. Bhutto, B. Q. Mercado, P. L. Holland, *Inorg. Chem.* **2023**, *62*, 9335–9342.
- [25] S. M. Bhutto, R. X. Hooper, S. F. McWilliams, B. Q. Mercado, P. L. Holland, *Chem. Sci.* **2024**, Advance Article.
- [26] B. K. Bower, H. G. Tennent, *J. Am. Chem. Soc.* **1972**, *94*, 2512–2513.
- [27] R. A. Lewis, D. E. Smiles, J. M. Darmon, S. C. Stieber, G. Wu, T. W. Hayton, *Inorg. Chem.* **2013**, *52*, 8218–8227.
- [28] A. Casitas, J. A. Rees, R. Goddard, E. Bill, S. DeBeer, A. Fürstner, *Angew. Chem. Int. Ed.* **2017**, *56*, 10108–10113.
- [29] R. A. Lewis, G. Wu, T. W. Hayton, *J. Am. Chem. Soc.* **2010**, *132*, 12824–12816.

- [30] P. G. N. Neate, B. Zhang, J. Conforti, W. W. Brennessel, M. L. Neidig, *Org. Lett.* **2021**, *23*, 5958–5963.
- [31] CCDC Deposition numbers 2331539 (for **1**), 2331540 (for **2**), and 2331541 (for **3**) contain the supplementary crystallographic data for this paper. These data are provided free of charge by the joint Cambridge Crystallographic Data Centre and Fachinformationszentrum Karlsruhe Access Structures service.
- [32] Q. Liang, J. H. Lin, J. C. Demuth, M. L. Neidig, D. Song, *Dalton Trans.* **2020**, *49*, 12287–12297.
- [33] U. Chakraborty, A. Fedulin, A. Jacobi von Wangelin, *ChemCatChem*. **2022**, *14*, e202201105.
- [34] M. M. Olmstead, P. P. Power, S. C. Shoner, *Inorg. Chem.* **1991**, *30*, 2547–2551.
- [35] M. P. Crockett, A. S. Wong, B. Li, J. A. Byers, *Angew. Chem. Int. Ed.* **2020**, *59*, 5392–5397.
- [36] D. E. DeRosha, V. G. Chilkuri, C. Van Stappen, E. Bill, B. Q. Mercado, S. DeBeer, F. Neese, P. L. Holland, *Nat. Chem.* **2019**, *11*, 1019–2015.
- [37] F. Neese, *Inorg. Chim. Acta.* **2002**, *337*, 181–192.
- [38] S. Ye, E. Bill, F. Neese, *Inorg. Chem.* **2016**, *55*, 3468–3474.
- [39] C. Lu, E. Bill, T. Weyhermüller, E. Bothe, K. Wieghardt, *J. Am. Chem. Soc.* **2008**, *130*, 3181–3197.
- [40] J. Bernauer, J. Polker, A. Jacobi Von Wangelin, *ChemCatChem*. **2022**, *14*, e202101182.
- [41] S. Ganguly, L. J. Giles, K. E. Thomas, R. Sarangi, A. Ghosh, *Chemistry*. **2017**, *23*, 15098–15106.
- [42] D. Shimizu, A. Osuka, *Chem. Sci.* **2018**, *9*, 1408–1423.
- [43] F. Neese, F. Wennmohs, U. Becker, C. Riplinger, *J. Chem. Phys.* **2020**, *152*, 224108.
- [44] J. W. Furness, A. D. Kaplan, J. Ning, J. P. Perdew, J. Sun, *J. Phys. Chem. Lett.* **2020**, *11*, 8208–8215.
- [45] E. Caldeweyher, C. Bannwarth, S. Grimme, *J. Chem. Phys.* **2017**, *147*, 34112.
- [46] S. Ehlert, U. Huniar, J. Ning, J. W. Furness, J. Sun, A. D. Kaplan, J. P. Perdew, J. G. Brandenburg, *J. Chem. Phys.* **2021**, *154*, 61101.
- [47] F. Weigend, R. Ahlrichs, *Phys. Chem. Chem. Phys.* **2005**, *7*, 3297–3305.
- [48] V. Barone, M. Cossi, *J. Phys. Chem. A* **1998**, *102*, 1995–2001.
- [49] R. Bjornsson, F. Neese, S. DeBeer, *Inorg. Chem.* **2017**, *56*, 1470–1477.
- [50] S. Sinnecker, L. D. Slep, E. Bill, F. Neese, *Inorg. Chem.* **2005**, *44*, 2245–2254.

Manuscript received: March 14, 2024

Accepted manuscript online: June 12, 2024

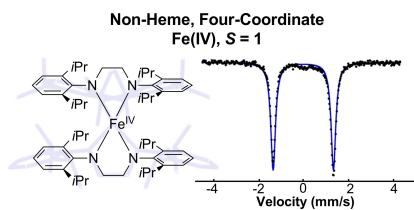
Version of record online: ■■■■■

Communication

Coordination Chemistry

B. Zhang, J. P. Joyce, N. J. Wolford,
W. W. Brennessel, S. DeBeer,
M. L. Neidig* [e202405113](#)

Unusual $S=1$ Four-Coordinate Fe(IV) Complexes Supported by Bisamide Ligands: Syntheses, Characterization, and Electronic Structures



In this study, we report the synthesis, spectroscopic characterization, and electronic structures of a pair of unusual $S=1$ non-heme four-coordinate formally Fe(IV) complexes, FeDipp₂ and FeMes₂, for which modifications of the aryl substituents of the bisamide ligands resulted in substantial structural changes and distinct bonding behaviors.